ADVANCED ENGINEERING MATERIALS

DOI: 10.1002/adem.201500371

Adhesion of Volcanic Ash Particles under Controlled Conditions and Implications for Their Deposition in Gas Turbines**

By *Catalina Taltavull, James Dean* and *Trevor William Clyne**

A particular (representative) type of ash has been used in this study, having a particle size range of ~10–70 μm. Experimental particle adhesion rate data are considered in conjunction with CFD modeling of particle velocities and temperatures. This ash becomes soft above ~700 °C and it has been confirmed that a sharp increase is observed in the likelihood of adhesion as particle temperatures move into this range. Particle size is important and those in the approximate range 10–30 μm are most likely to adhere. This corresponds fairly closely with the size range that is most likely to enter a combustion chamber and turbine.

1. Introduction

It is increasingly clear that gas turbines, particularly aero-engines, are susceptible to damage caused by ingested particulate, such as sand, fly ash, and volcanic ash, often referred to generically as calcia–magnesia–alumina–silica (CMAS). Such particles may melt, or at least soften, in flight, making it more likely that, if they strike solid surfaces within the turbine, they will adhere to them on impact. Ongoing increases in turbine entry temperature clearly raise the danger of this happening and there is particular concern about volcanic ash,[1–6] which often has a relatively low softening temperature.[4,7,8]

Adhesion of such particulate can lead (at relatively high levels) to disruption of gas flow through the engine, ranging from the blockage of cooling channels[9,10] to complete inhibition of air passage and combustion. At lower levels, short- or medium-term damage can be caused to protective ceramic coatings, with a particular danger of promoting spallation.[11–18] These effects are potentially of major concern, but they all depend on the likelihood of particle adhesion, with the sensitivity to this factor being much greater than that to the particulate burden of the ingested air. This can be seen by recognizing that, even at the particle concentration currently classed as "safe" by the CAA ($2\,mg\,m^{-3}$), the ingestion rate for a large turbofan engine at full power is more than $1\,g\,s^{-1}$. Since, even in a large engine, 1 g of adhered particulate (≈100 million particles of radius 10 μm) is likely to cause extensive damage, it is very clear that the critical factor here is the proportion of ingested particles that adhere to solid surfaces inside the engine.

The particle temperature on impact is clearly a key parameter, although the substrate temperature, roughness, and motion can also be important. Lower deposition rates are observed on cooler[19] and smoother[20] surfaces. It has also been noted[4,21] that deposition rates are much higher on static surfaces, such as platforms and guide vanes, than on rotating components, such as blades. It is also evident that, in addition to thermal effects, momentum-related factors influence the likelihood of particle impact on solid surfaces (stationary or moving). As with its thermal history, the size of the particle plays a key role. The factors dictating whether a particle carried in a fluid will strike an obstacle located in the stream, or pass around it, are well-established and are encapsulated[4,22–24] in

[*] *Dr. C. Taltavull, Dr. J. Dean, Prof. T. W. Clyne*
Department of Materials Science and Metallurgy, Cambridge University, 27 Charles Babbage Road, Cambridge CB3 0FS, UK
E-mail: twc10@cam.ac.uk

[**] *This work forms part of a research programme funded by EPSRC (EP/K027530/1). In conjunction with this project, a consortium of partners has been set up under the PROVIDA ("PROtection against Volcanic ash Induced Damage in Aero-engines") banner and information about its operation is available at http://www.ccg.msm.cam.ac.uk/initiatives/provida. The invaluable assistance of Kevin Roberts (Materials Department in Cambridge) with operation of the plasma spray facility is gratefully acknowledged. The authors are also grateful to Dr. Margaret Hartley, of the University of Manchester, for kindly collecting the Laki ash (and several other types) during field trips to Iceland, which were funded by EasyJet. In compliance with current EPSRC requirements, input data for the modeling described in this paper, including meshing and boundary condition specifications, are available at the following URL: www.ccg.msm.cam.ac.uk/publications/resources. These files can be downloaded and used in COMSOL Multiphysics packages. Data supplied are for a representative case.*

the Stokes number, which is the ratio of the characteristic time for velocity change to that for passing the obstacle. The magnitude of the Stokes number is plotted in Figure 1, as a function of particle diameter, with the other parameters given values broadly appropriate for the passage of ash particles through a turbine. When $Stk >> 1$, impact is expected, while for $Stk << 1$ the particle will be carried around the obstacle with the fluid stream. It can be seen in the plot that particles less than about 2–3 μm in diameter are expected to miss (stationary) obstacles, while those larger than about 5–7 μm will strike them. For intermediate sizes, the situation is less clear-cut and factors such as the exact shapes of particle and obstacle may be relevant. Systematic experimental data are required in this area.

In view of both thermal and momentum-related effects,[19] there is considerable interest in the size distribution of particles ingested with the air intake (of an aero-engine). The maximum size of particles ingested into a jet engine has been reported[25,26] to be about 100 μm. It is, however, worth noting that the size distribution of particles entering the air intake may differ significantly from that of particles entering the turbine, as a consequence of relatively large particles being both centrifuged into the bypass air flow and fragmented by impact with compressor blades. There appears to be very little published information[27] about these effects, for any type of gas turbine, although Weaver et al.[28] do refer to their samples (having average sizes ranging from 5 to 15 μm) as being "... consistent with distributions measured at the exit of high compressors for large turbofan engines." In general, it seems likely that particles larger than about 30 μm in diameter do not commonly enter the combustion chamber or reach the turbine. Much of the interest therefore centers on the size range from a few microns to a few tens of microns, since particles below this range rarely strike solid surfaces, while larger ones rarely enter the turbine.

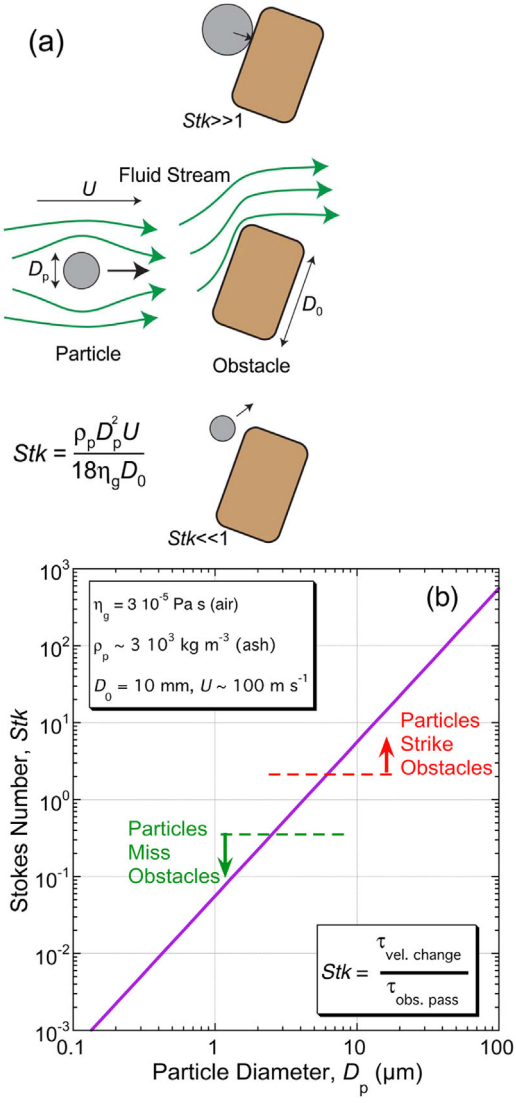

Fig. 1. (a) Schematic showing how the magnitude of the Stokes number controls particle flight paths in a fluid and (b) influence of particle size on the Stokes number, for values of the other parameters appropriate to passage of VA through a turbine.

The current study involves injection of a particular type of ash, containing particles in this size range of interest, into a set-up designed to simulate passage through a combustion chamber and subsequent projection toward a solid surface, inclined at pre-selected angles to the overall flow direction. The deposition rate is measured, as a function of the thermal and velocity fields of the gas stream, with a view to obtaining insights into the key features of a volcanic ash particle that dictate whether it is likely to adhere to a solid surface on impact.

2. Experimental Section

2.1. Powder Characterization

The volcanic ash (VA) was extracted near the Laki vent in Southern Iceland. (The Laki explosions, in 1783–1784, are among the largest in historical times and are estimated to have created about a hundred times as much ash as the eruptions of Eyjafjallajökull in 2010.) The as-received ash was ground in a rotary mill and then passed through a sieve with a spacing of the order of 40 μm. The chemical composition, obtained from EDX data, is shown in Table 1. It can be seen that the ash contains a number of elements at significant levels, and is particularly rich in Si and Fe. The phase constitution of this VA was investigated via X-ray diffraction. The spectrum, published previously,[4] shows four crystalline phases, all at relatively low levels, with a prominent broad peak at ≈20–30° (2θ), signifying a substantial proportion (≈80%) of amorphous phase.

The glass transition temperature and "melting point" of the VA were obtained with the set-up shown in the insert in Figure 2, using a Netzsch 402C dilatometer. (This has been found to be more accurate and reliable than the commonly used DSC procedure, although that gave similar results in the current case.) A cold isostatic press was used to fabricate a "green" cylindrical pellet of VA, about 5 mm in diameter and 1.5 mm in length. This specimen was placed in an alumina crucible and an alumina push rod applied a constant load of 0.3 N to the specimen, which was heated at 5 °C min^{-1}. Initially, the powder compact expands on heating, but then a

ADVANCED ENGINEERING MATERIALS 2015,
DOI: 10.1002/adem.201500371

Table 1. Elemental composition of the VA powder, obtained by EDX analysis.

Element	Weight [%]
O	Bal.
Na	1
Mg	2
Al	6.7
Si	24
K	0.1
Ca	6.1
Ti	2.4
Fe	21.3

contraction is observed (on passing through the glass transition temperature, T_g) as the amorphous fraction softens dramatically, so that powder particles start to deform and the compact becomes denser. This contraction accelerates when the particles finally melt. It can be seen from the plot in Figure 2 that T_g is ≈650–700 °C and the melting point, T_m (temperature at which the crystalline phases melt) is ≈1 050–1150 °C. Of course, the concept of a T_m value is slightly dubious here, since there is only a small crystalline content (comprising several phases). Nevertheless, the observed behaviour is fairly clear and these characteristics are also consistent with DSC measurements made previously[4] on the same ash, which also revealed the specific heat of the powder to be ≈800 J kg^{-1} K^{-1}.

The particle size distribution of the powder was obtained using a Malvern P580 Mastersizer E. The powder was dispersed in water and kept in suspension using a stirrer. The outcome is shown in Figure 3a, where it can be seen that the average particle size (diameter) was ≈30 μm, with most particles in the range 5–70 μm. Particle morphologies were examined using a JEOL-5800 SEM, with an accelerating voltage of 10–15 kV. Samples were sputter coated with gold, to prevent charging. Typical morphologies were observed to be angular and irregular—see Figure 3b.

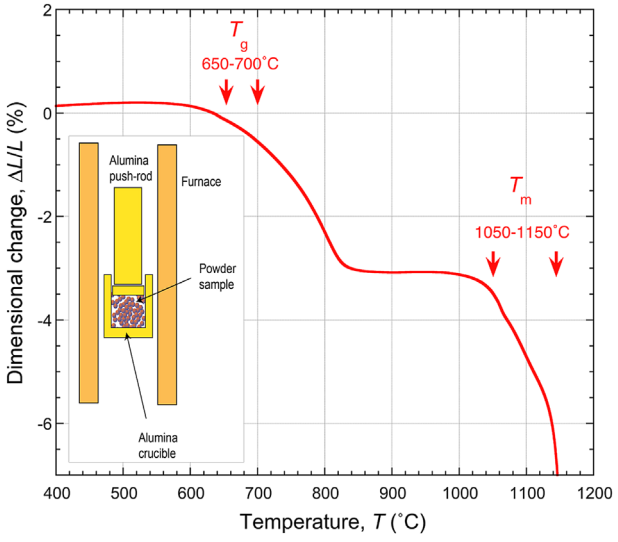

Fig. 2. Fractional length change, as a function of temperature, for a compacted powder sample, obtained using a heating rate of 5 °C min^{-1}.

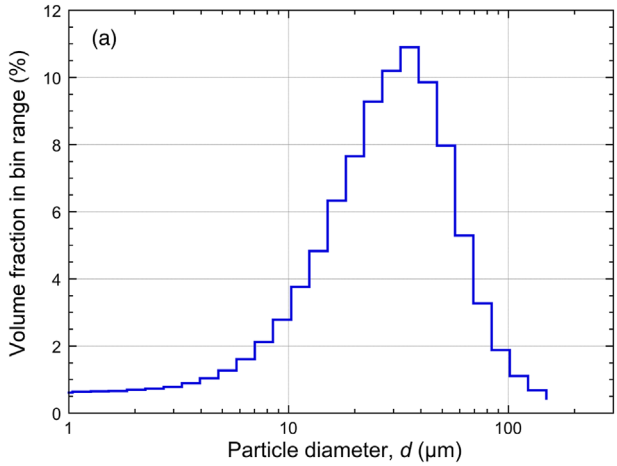

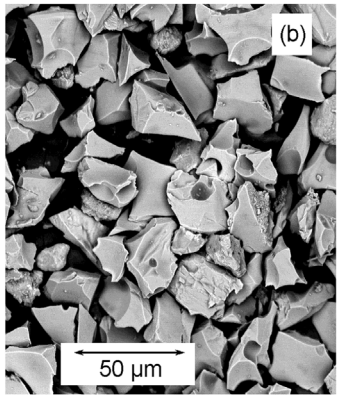

Fig. 3. Particle size and shape range of the powder used, illustrated by: (a) a size distribution plot and (b) an SEM micrograph.

Since this VA is partially crystalline, and T_g is well below the crystal melting temperatures, the distribution of phases between the particles is of interest. Information about this is provided in Figure 4, which shows an SEM image and elemental composition maps from a polished section containing a number of particles. Many of the particles are fully amorphous, but some do contain dispersed crystalline phases.

No attempt has been made to identify any of those in this section, but it can be seen that there is quite pronounced elemental partitioning between the phases. For example, much of the Fe appears to be in crystalline phases, which include[4] magnetite (Fe_3O_4). In general, however, most of the particles appear to be at least partially amorphous, and so are expected to become soft, if not fully molten, as their temperature rises above T_g. This is potentially significant, since, for this VA (and for many others), the glass content is high and T_g is several hundred °C below what is commonly[8,29,30] taken to be the "melting temperature" of VAs, which is usually ≈1 100–1 200 °C. (The current Wikipedia entry under "Volcanic Ash and Aviation Safety" states: "Volcanic Ash has a Melting Point of approximately 1 100°C.") In fact, it is already clear that both the glass content and the T_g

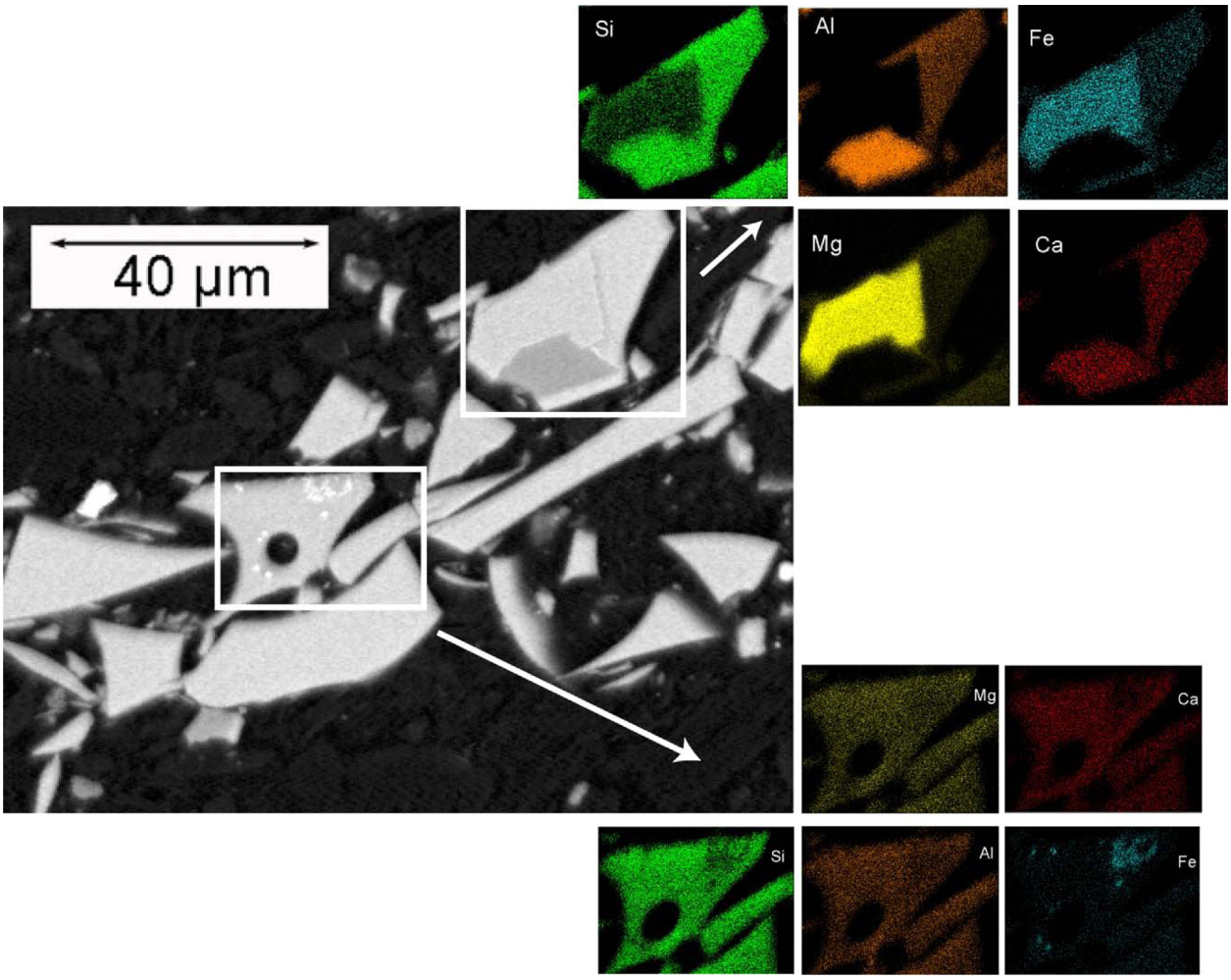

Fig. 4. SEM micrograph of a polished section of particles mounted in resin, together with EDX element maps from the two regions shown.

value can vary substantially from one volcanic source to another (even in the same geographic area). This is not really surprising, since these factors are highly sensitive (in a way that is very difficult to predict in detail) to the nature of the coordination polyhedra that form in the atomic scale structure, and hence to the precise composition.

2.2. Process Conditions

A systematic study of the factors affecting adhesion of VA particles requires a set-up in which relevant parameters (particularly velocity and temperature fields of the gas, plus temperature, roughness and orientation of the substrate surface) can be properly controlled. Also, it is clearly important to be able to measure the proportion of incident particles that adhere. While there are evidently attractions in using real jet engines (or other gas turbines) for adhesion experiments of this type, these issues inevitably lead to a requirement for some kind of simulation arrangement. In the current work, a vacuum plasma spray system (Plasma-Technik unit with an F4 gun and 7 mm nozzle) has been used, with chamber pressure, plasma power and powder feed rates adjusted as appropriate. The conditions generated in such a system are not very close to those in the combustion chamber of a gas turbine, particularly in terms of gas pressure (which was well below one bar in these experiments, compared with up to 40 bar in a combustion chamber). However, a key objective is to study the sensitivity of the probability of adhesion to parameters such as particle temperature and velocity at impact. Such information, acquired via experiments of the type described here, can then be used to predict the behaviour under conditions in a real engine.

The experimental arrangement is depicted schematically in Figure 5. The stainless steel tube (550 mm long and 80 mm in diameter) provided an environment simulating (at least approximately) that of a combustion chamber. A W-type thermocouple was located 175 mm from the nozzle and K-types were placed at 340 and 500 mm. Axial gas velocities were established using a Pitot tube type L (Kimo Instruments), placed at distances of 350 and 450 mm, the latter being the standard location of the substrate. Three different sets of operating conditions were employed (A, B, and C), as shown in Table 2. Measured gas temperatures and velocities (Table 2) were used for setting up the CFD model (see Section 3.1).

DOI: 10.1002/adem.201500371

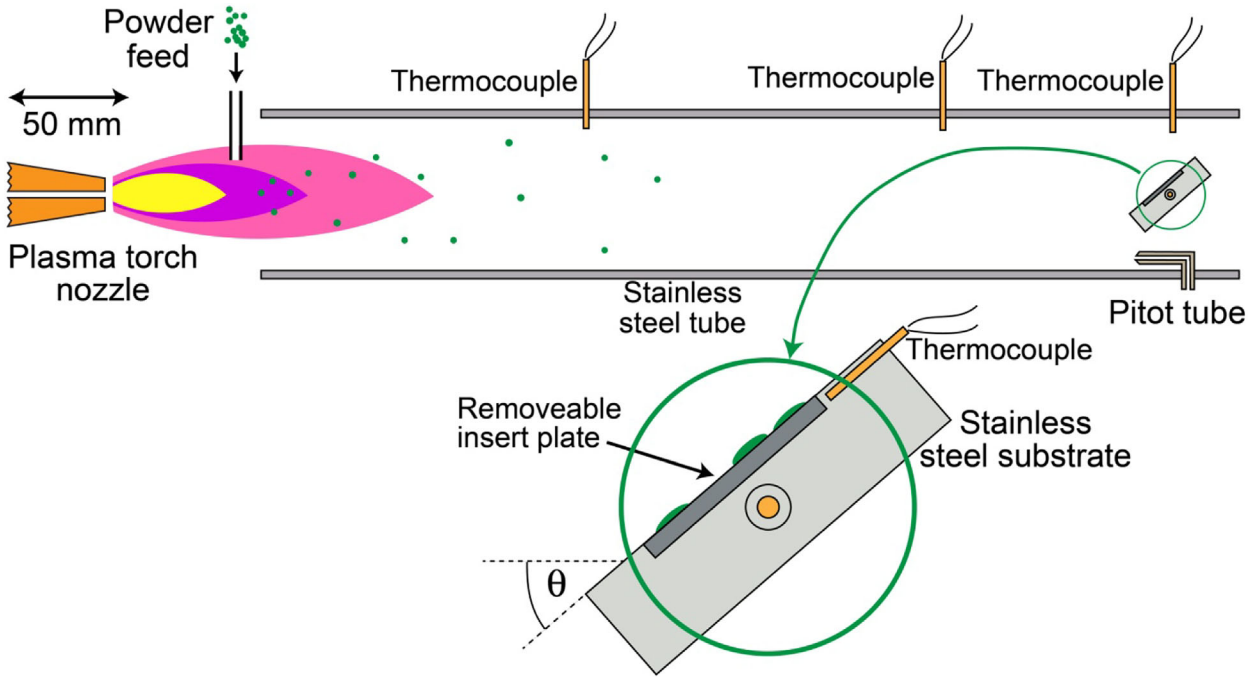

Fig. 5. Schematic representation of the experimental set-up for monitoring of particle deposition rates, based on a plasma torch located within a vacuum chamber.

Table 2. Sets of operating conditions employed in the tests.

			Temperatures [°C]							
			Gas at x [mm]			Substrate ($x = 450$ mm)			Speeds [m s^{-1}] at x [mm]	
Case code	Chamber pressure [mbar]	Plasma power [kW]	175	340	500	$\theta = 90°$	$\theta = 60°$	$\theta = 30°$	350	450
A	120	30	1115	839	770	410	404	429	92.2	90.6
B	100	35	1415	970	885	526	528	560	106.8	105.9
C	80	40	1932	1143	1022	600	621	659	127.5	126.9

2.3. Injection of Ash Particles and Measurement of Deposition Rates

After the system had stabilized under the selected set of conditions (usually about 30 s), VA powder was injected into the region slightly in front of where the plasma plume exits the nozzle[†] (Figure 5), at a predetermined rate (using the powder feed unit supplied with the plasma spray system). The injection rate was fixed (at 34.3 mg s^{-1}) and the injection period was also standardized (at 10 s). The quantity of powder injected was therefore the same in all cases (343 ± 30 mg). Deposition rates were established by weighing the insert in the substrate before and after each experiment. The dimensions of substrate and inserts were respectively $50 \times 30 \times 18$ mm and $40 \times 20 \times 1.7$ mm. The mass of an insert was thus about 11–12 g. Weight gains after deposition were of the order of 2–30 mg. These are relatively small changes in overall insert mass (≈0.02–0.3%), but the balance used (Leco-250) had a precision of ±50 μg and the error on these measured mass gains is probably <10%, particularly for the higher deposition rates.

In order to establish the fraction of particles (initially incident on the insert) that adhere to it, an assumption must be made regarding the spatial distribution of the injected particles across the section of the tube. This was checked by prolonged injection experiments in which substrates were placed at various locations in the section, using thermal conditions such that most particles "melted" and then adhered to the substrates. In this way, it was confirmed that, at least toward the end of the

[†] It may be noted that, while there is a genuine plasma inside the nozzle, where the arc is created, virtually no charged particles are present in the plume outside of the nozzle. Furthermore, while the core of the plasma is very hot (up to 10 000 or 20 000 K), both temperature and velocity drop off sharply (depending to some extent on the chamber pressure) on exiting the nozzle and in general the plume in this region is sub-sonic and no hotter than about 3 000 K. Of course, both temperature and velocity continue to fall off with distance from the nozzle.

tube, the injected particles had become uniformly distributed throughout the sectional area. This meant that a fraction f of the injected particles were being projected toward the insert as they approached the substrate, given by

$$f = \frac{Lb\sin\theta}{\pi R^2} \quad (1)$$

where L and b are the in-plane dimensions of the insert and R is the inner radius of the tube. Since L was 40 mm, b was 20 mm, and R was 40 mm, with θ values of 90°, 60°, and 30°, corresponding f values were 15.9, 13.8, and 7.96%. For all of the cases presented here, the inserts were uncoated (stainless steel), ground to 1 200 grit finish. The weight data obtained, for the three different sets of thermal conditions (A, B, and C), and for three different values of the substrate inclination angle, θ, are presented in Table 3. The values in the column headed "projected at insert" are the products of the injected mass of particulate (343 mg in all cases) and the values of f for the substrate orientation angles concerned.

3. CFD Modeling of Particle Acceleration, Heating, and Impact

3.1. Model Formulation and Boundary Conditions

CFD simulations were carried out using the COMSOL Multiphysics package. Experimentally measured thermal fields (for Cases A, B, and C) were imposed on the gas (argon), using analytical functions. Temperature dependences of gas viscosity, thermal conductivity, and specific heat were taken into account. Gas density was dependent on both temperature and pressure. The initial pressure was set to the values in Table 2.

The turbulence model employed was the Reynolds-Averaged Navier Stokes (RANS) type, using the k–ε turbulence model, and wall functions were used to model the region close to the walls, where there are large gradients in flow parameters. An inlet velocity boundary condition was specified at the entrance to the tube. This velocity was altered iteratively until the predicted velocity field agreed closely with experimental data. A pressure outlet boundary condition was specified at the tube exit, consistent with the overall pressure in the chamber (which was being dynamically maintained by the pumping system). These chamber pressure values, for Cases A, B, and C, are shown in Table 2.

Flow field simulations were coupled with the imposed thermal field, using the COMSOL conjugate heat transfer multi-physics interface. This coupling was one-way, such that the flow characteristics were affected by the temperature field, but there was no interaction in the reverse direction. Once a solution had been obtained for the flow field, a particle tracing interface was added to the model. Single (spherical) particles (of varying size) were injected at the inlet to the tube (along its centerline), with an initial velocity of 1 m s^{-1} and an initial temperature of 20 °C.

Central to the dynamics of particles in fluids are values of the drag coefficient. Particle shape (see Figure 3b) was taken into account, since this can strongly influence drag coefficients in high Reynolds number flows.[31] (The value of Re in these experiments was of the order of 10^4.) The shape effect was characterized in terms of the deviation from that of a perfect sphere by measuring the particle "sphericity," which is simply related to the ratio of volume and surface area. A few μg of VA

Table 3. Weight gain data.

	Substrate inclination		Mass [mg] Insert				
Case code	θ [°]	f [%]	Initial	Final	Gain	Projected at insert	Fraction deposited W [%]
A	90	15.9	12 131.5	12 137.3	5.8	54.5	10.6
	90	15.9	12 028.4	12 035.1	6.7	54.5	12.3
	60	13.8	11 307.3	11 311.0	3.7	47.3	7.8
	60	13.8	12 113.4	12 116.5	3.1	47.3	6.6
	30	7.96	12 067.3	12 068.7	1.4	27.3	5.1
	30	7.96	12 111.9	12 112.9	1.0	27.3	3.7
B	90	15.9	12 141.3	12 153.1	11.8	54.5	21.6
	90	15.9	12 069.7	12 080.7	11.0	54.5	20.2
	60	13.8	11 340.7	11 349.0	8.3	47.3	17.6
	60	13.8	12 106.7	12 116.5	9.8	47.3	20.7
	30	7.96	11 384.5	11 388.0	3.5	27.3	12.8
	30	7.96	12 055.4	12 058.5	3.1	27.3	11.3
C	90	15.9	12 049.5	12 072.0	22.5	54.5	41.2
	90	15.9	12 089.6	12 118.5	28.9	54.5	53.0
	60	13.8	11 360.9	11 381.2	20.3	47.3	42.9
	60	13.8	12 083.1	12 096.1	13.0	47.3	27.5
	30	7.96	12 057.5	12 065.3	7.8	27.3	28.5
	30	7.96	12 104.0	12 107.7	3.7	27.3	13.5

DOI: 10.1002/adem.201500371

powder was sprinkled onto a sample holder and analyzed by Computed X-Ray Micro-tomography, with a scan resolution of ≈1 μm. Particles in the size range of prime interest (≈25 μm) were 3D-rendered using Simpleware ScanIP reconstruction software. A total of 20 particles were reconstructed in this way. Their average sphericity was 0.73. This value was used in the Haider–Levenspiel drag law relationship that is available in the COMSOL suite. Gravitational effects were included, although their influence is small for most cases of interest (i.e., for particle sizes below about 50 μm).

Another key parameter is the heat transfer coefficient for the particle-gas interface, h_i, which is the proportionality constant relating temperature difference (between particle surface and nearby gas) to heat flux. While this formulation is common, it must be recognized that it encapsulates several effects. The value of h_i is affected by the thickness, δ, of the interfacial boundary layer in the gas, and in fact it can be approximated to k_g/δ, where k_g is the gas conductivity. However, prediction of either h_i or δ is complex, since they depend on several variables, including gas composition, pressure and density, particle size and relative velocity between particle and gas. Furthermore, since the particles are taken to be spherical, the thermal effects of the actual particle shape must be incorporated into the value of h_i.

There are various theoretical treatments available[32,33] for prediction of h_i, which can be applied over a range of velocity and particle size, but most systematic experimental measurements[34] tend to concern lower velocities and larger particles than for the present case. Semi-empirical correlation expressions are available and have been applied[35] to the regime of high relative velocities and small particles. These analyses suggest that, for velocities in the range 10–100 m s^{-1}, an h_i value around 10 kW m^{-2} K^{-1} is appropriate for small (few μm) particles in argon, but that figure falls to around 1-3 kW m^{-2} K^{-1} for particles in the 10–50 μm size range, which is of prime interest here. Recognizing that these particular experiments involve argon at reduced pressure (≈100 mbar), an h_i value of 1 kW m^{-2} K^{-1} has been selected as a default, taken as constant (independent of relative velocity and particle size). This is a relatively crude approximation, on which it should be possible to improve in future work, but it is considered acceptable for present purposes. (A higher value would probably be appropriate within a combustion chamber, where the gas pressure is much higher, and some model predictions are shown that illustrate the effect of an increase.)

One point that can be noted at this juncture is that the magnitude of the Biot number, *Bi*, is therefore small (<<1). The value of *Bi* (ratio of the thermal conductance of the interface to that of the interior of the particle), which is given approximately by $(h_i R)/k_p$, where k_p is the conductivity of the particle (measured for this material[4] to be ≈2 W m^{-1} K^{-1}), varies from about 10^{-3} to 10^{-1} over a particle size range from 1 to 100 μm. Thus, for all cases being considered here, individual particles are approximately isothermal throughout and there is no need to model the heat flow within them.

3.2. Gas Temperature and Velocity Fields

Modeling runs have been carried out for the three cases listed in Table 2, with boundary conditions set so as to give good agreement with the (steady state) experimental measurements of gas temperature and velocity, as well as conforming to the pre-set value of the chamber pressure. Comparisons are presented in Figure 6a and b between modeled and measured thermal and velocity fields (along the tube axis) for the three cases. It can be seen that the modeled fields are broadly consistent with the experimental data. Figure 6c shows a contour map of gas velocity (for an inclined substrate), giving an indication of the nature of the disturbance introduced by the presence of the substrate.

3.3. Particle Temperature and Velocity Histories

Injection of particles into the gas stream was assumed to have a negligible effect on its behaviour. Thermal histories of

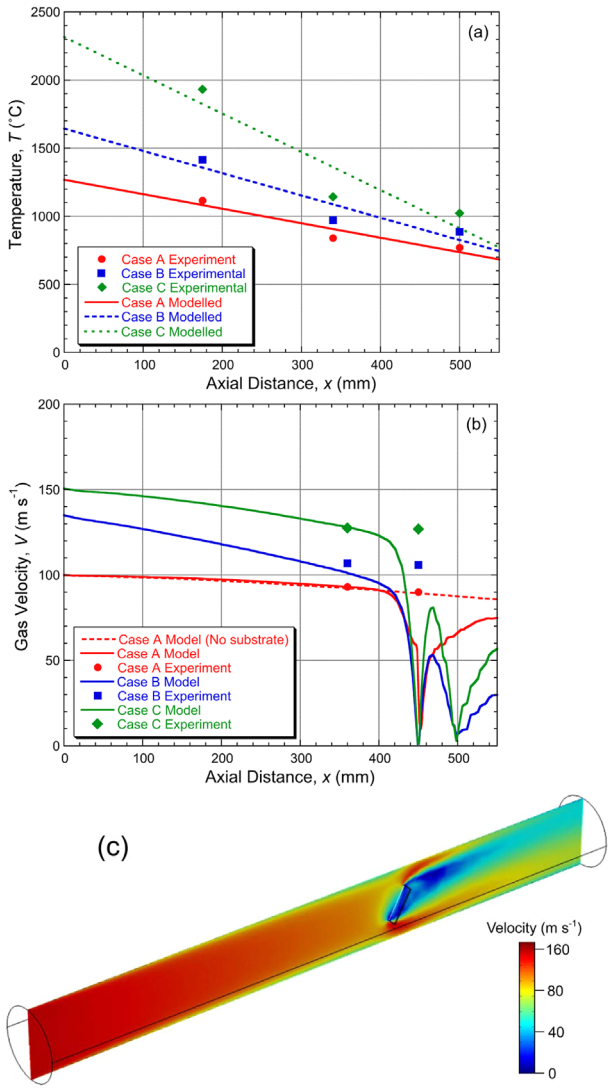

Fig. 6. Experimental and modeled thermal and velocity fields of the gas, showing axial profiles for the three cases, with θ = 90°, of (a) temperature and (b) velocity, while (c) is a velocity contour map in the (vertical) x–r plane, for Case C, with θ = 60°, illustrating the perturbations caused by the substrate.

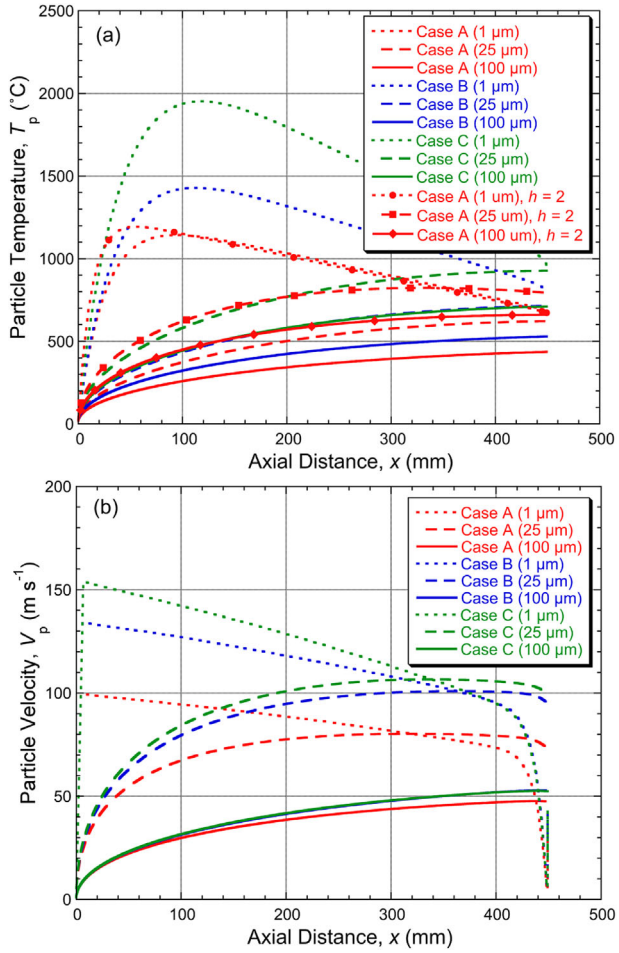

Fig. 7. Predicted variations (for $\theta = 90°$) of: (a) particle temperature and (b) particle velocity, as a function of distance along the axis of the tube, for the three processing condition cases and for three particle sizes. In (a), most data refer to an h_i value of 1 kW m^{-2} K^{-1}, but plots are also shown (for Case A) illustrating the effect of raising this to 2 kW m^{-2} K^{-1}.

(spherical) particles injected into the gas stream along the tube axis are shown in Figure 7a, for three different particle sizes and for the three process condition cases.

Of course, the particle size has a strong effect, with 1 μm particles quickly coming close to the neighboring gas temperature, while the larger particles always lag behind considerably. However, the temperature of 25 μm particles is close to that of the surrounding gas by the time that they reach the substrate (whereas the 100 μm particles still lag behind at that point). Also shown is a set of plots for which the heat transfer coefficient value has been doubled. It can be seen that this does have a significant effect (for the larger particles) and it is clear that the details of the gas-particle heat transfer are likely to be important.

Particle velocity histories are shown in Figure 7b. Again, small particles conform more closely to the velocity of the adjacent gas, and in fact the 1 μm particles reach the gas velocity within just a few mm of the injection point. Larger particles are accelerated more slowly, but the 25 μm particles have again reached a similar speed to that of surrounding gas by the time they reach the vicinity of the substrate. Of course, these velocities (along the axis of the tube), and those of the gas, fall sharply as the substrate is approached, particularly for the small particles. In practice, the substrate inclination angle, and the component of the particle velocity normal to the substrate surface, are likely to be important in terms of the nature and effect of the impact. This is examined in Section 4.2.

4. Powder Injection and Deposition

4.1. Observed Deposition Behaviour

As expected, the rate of particle adhesion rose as the plasma power was increased (raising the gas temperature and velocity). There were also some changes in the appearance of individual splats. This is illustrated by Figure 8, which shows SEM micrographs of insert surfaces (all for normal incidence, $\theta = 90°$). Clearly, the spatial density of splats increases as conditions become more severe. There is also evidence of more complete spreading of individual splats at the higher gas (and substrate) temperatures, although this is somewhat complicated by the relatively wide range of particle sizes, and also by the fact that the behaviour changes somewhat as the coverage increases and the surface becomes rougher. In any event, it is clear that the likelihood of adhesion is raised as particles become hotter (and hence softer).

It is evidently important to attempt at least semi-quantitative analysis of this effect. Figure 9 shows measured adhesion rates for the three different sets of processing conditions, and for the three inclination angles (characterized by the corresponding substrate temperatures). While some scatter is inevitable with such measurements, adhesion rates clearly do rise as gas (and hence particle and substrate) temperatures increase and it is also clear that lower impact angles lead to appreciably lower adhesion rates (over the complete range of substrate temperature).

4.2. Correlation with Modeled Impact Characteristics

A correlation is shown in Figure 10a between adhesion rates (for normal incidence) and particle temperature at impact, for a range of particle size. It is worth noting at this point that measured weight gains are influenced more strongly by the behaviour of the larger particles. (For example, one 50 μm particle weighs the same as a thousand 5 μm particles.) In view of the PSD of the powder used (Figure 3a), particles in the approximate diameter range of 20–50 μm are likely to dominate these measurements, although, in a real engine, it is probably the range 5–30 μm that is of most interest. Focusing on the 20–50 μm size range in Figure 10a, it can be seen that deposition rates start to rise sharply as these particles start to reach temperatures (on impact) of ≈700–900 °C. This correlates well with the data shown in Figure 2, where it can be seen that this is the range just above T_g, where, given the high glassy content of this VA, at least most of these particles are expected to become very soft. It is clearly not necessary for particles to reach temperatures close to or above

ADVANCED ENGINEERING MATERIALS 2015,
DOI: 10.1002/adem.201500371

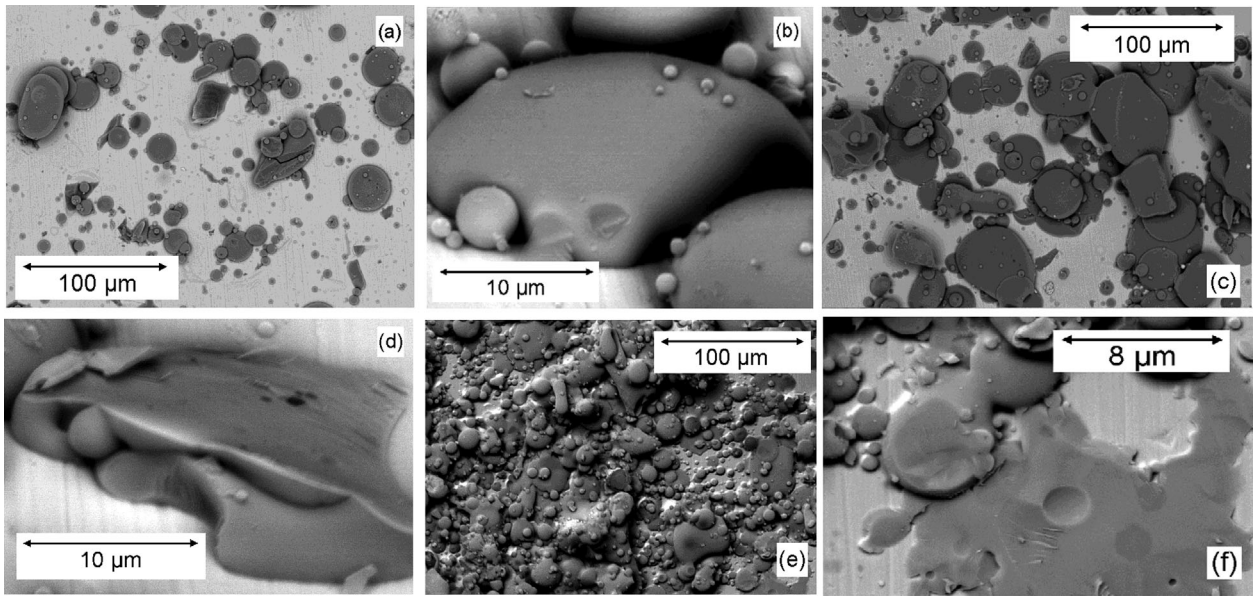

Fig. 8. SEM micrographs of insert surfaces, with adhering VA splats, after powder injection for 10 s, with normal incidence ($\theta = 90°$), under (a) and (b) Case A conditions, (c) and (d) Case B conditions and (e) and (f) Case C conditions.

the "melting temperature," which in this case is about 1 100°C, for adhesion to occur.

Of course, there is also the important issue of how the particles strike the substrate (and parameters such as substrate surface roughness and temperature may also be relevant). This is the main factor for very fine particles, which probably do not strike substrates at all—see Figure 1. However, in the size range of prime interest (≈5–30 μm), the impact velocity, and in particular the velocity component normal to the substrate surface, is expected to have an effect—presumably even a very soft particle would be unlikely to adhere if it strikes a substrate only at grazing incidence. Information relating to this is presented in Figure 10b, where the adhesion data (for all three inclination angles) are correlated with values of the component of the particle velocity acting normal to the substrate surface, at the point of impact. These data are plotted for three particle sizes. It is clear that these values are low in all cases for the fine (1 μm) particles, which are carried (at high overall speed) by the gas stream, but are always expected to either miss the substrate or experience only grazing impact. Large (100 μm) particles, on the other hand, do strike the substrate, but, in addition to being relatively cold, they do not reach high speeds. At the intermediate (25 μm) size, however, higher impact velocities (≈30–50 m s^{-1} in this case) can be reached. It can be seen that there is an increase in velocity with increasing substrate temperature (i.e., with higher plasma power and reduced chamber pressure), but it is not very significant and it seems likely that the sharp rise in deposition efficiency as these changes are made is primarily due to the higher particle temperatures at impact (particularly as they start to exceed T_g).

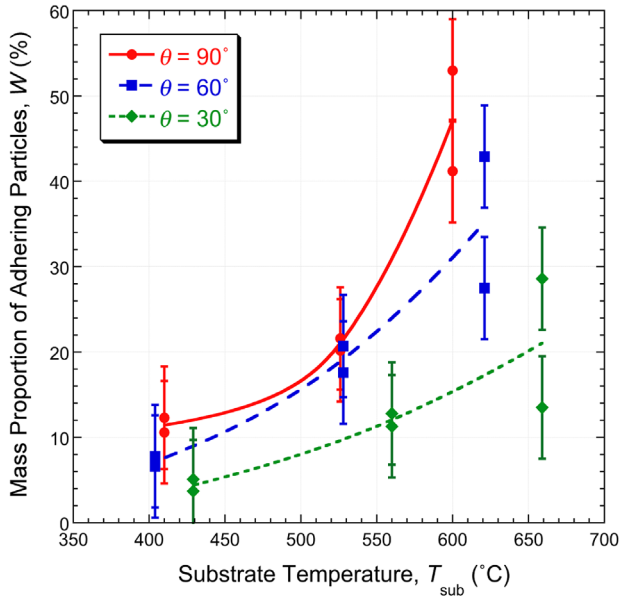

Fig. 9. Plot of the proportion of incident particles adhering to the insert, as a function of the substrate temperature.

It is clear that detailed study of impact, spreading, and adhesion requires modeling of the associated deformation process. Such processes have been analyzed[36–41] in some depth, but identifying appropriate input data for the mechanical properties of the material presents a major challenge, particularly since deformation occurs at very high strain rates (as well as high temperatures). For particles that are in some kind of semi-solid state, it is not even clear whether treatments should be based on viscous flow or plasticity models, although in both cases the strain rate (and temperature) dependence need to be taken into account. Nevertheless, even without such analysis, the present results give a clear indication that information about in-flight heat transfer to particles, and the temperature range in which

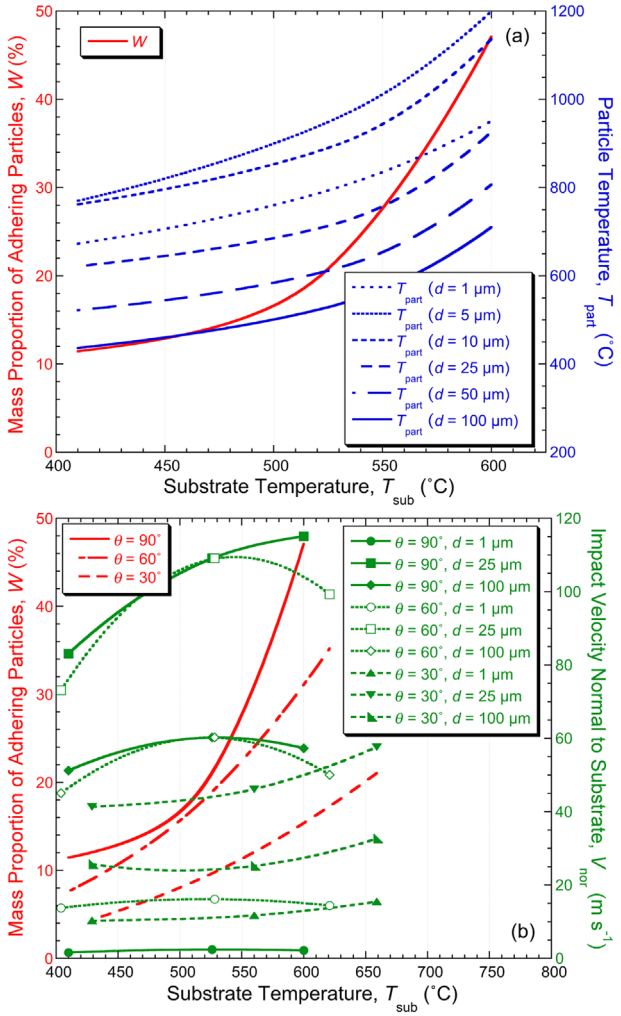

Fig. 10. Measured adhesion rates and predicted particle parameters at impact, as a function the processing conditions (represented by the substrate temperature), showing: (a) temperature, for normal incidence ($\theta = 90°$), and (b) component of the velocity normal to the substrate, for the three incident angles. The thermal histories were obtained using a heat transfer coefficient, h_i, of 1 kW m^{-2} K^{-1}.

major softening occurs, can provide a useful framework for assessment of the likelihood of adhesion.

5. Conclusions

The following conclusions can be drawn from this work.

1) Controlled environment experiments, representative, at least in some ways, of the combustion chamber of a gas turbine, have been used, in combination with CFD modeling, to obtain insights into the factors affecting adhesion of a typical volcanic ash to solid surfaces similar to those within a turbine. Measurements have been made of the mass proportion of incident ash particles that adhere to substrates in the gas stream, with experimental values being obtained up to about 50%.
2) Unsurprisingly, hotter particles, striking a substrate with large velocity components normal to its surface, are more likely to spread and adhere. More quantitatively, however, evidence is presented indicating that particles only need to be above their T_g value (about 700 °C in this case) in order to be likely to adhere. In this temperature range, which is well below the nominal melting point (≈1 100 °C), particles can apparently become sufficiently soft for deformation and adhesion to be likely. It is therefore important that the T_g value (and glass content) should be established for any VA giving cause for concern.
3) The behaviour depends strongly on particle size, as well as on the thermal and velocity fields of the gas in which it is carried. Size affects both the rate at which the particle temperature approaches that of surrounding gas and the nature of any impact with solid surfaces—with small (<≈2–3 μm) particles being unlikely to strike them at all. Large (>≈100 μm) particles would often fail to reach T_g, and in any event rarely enter combustion chambers. An intermediate size range (~10–30 μm) is probably of most concern.
4) It is been shown that the likelihood of a particle adhering to a substrate is influenced by the component of its impact velocity normal to the surface, although the deformation and adhesion behaviour is probably less sensitive to this factor (provided impact does occur) than to temperature—particularly in the vicinity of T_g. Detailed modeling of how particles deform and adhere on impact, as a function of these variables, may be helpful.

Article first published online: xxxx
Manuscript Revised: September 25, 2015
Manuscript Received: July 20, 2015

[1] J. Kim, M. G. Dunn, A. J. Baran, D. P. Wade, E. L. Tremba, *J. Eng. Gas Turbines Power (ASME)* **1993**, *115*, 641.
[2] C. Witham, H. Webster, M. Hort, A. Jones, D. Thomson, *Atmos. Env.* **2012**, *48*, 219.
[3] W. Ai, T. H. Fletcher, *J. Turbomach.* **2012**, *134*, 041020.
[4] M. Shinozaki, K. A. Roberts, B. van de Goor, T. W. Clyne, *Adv. Eng. Mats.* **2013**, *15*, 986.
[5] C. R. Davison, T. A. Rutke, *J. Eng. Gas Turbines Power (ASME)* **2014**, *136*, Article No. 081201.
[6] M. G. De Giorgi, S. Campilongo, A. Ficarella, *J. Eng. Gas Turbines Power (ASME)* **2015**, *137*, Article No. 052603.
[7] A. Hamed, W. Tabakoff, R. Wenglarz, *J. Propul. Power* **2006**, *22*, 350.
[8] W. J. Song, K. U. Hess, D. E. Damby, F. B. Wadsworth, Y. Lavallee, C. Cimarelli, D. B. Dingwell, *Geophys. Res. Lett.* **2014**, *41*, 2326.
[9] W. G. Ai, N. Murray, T. H. Fletcher, S. Harding, S. Lewis, J. P. Bons, *J. Eng. Gas Turbines Power (ASME)* **2012**, *134*, Article No. 041013.
[10] K. Brun, M. Nored, R. Kurz, *J. Eng. Gas Turbines Power (ASME)* **2012**, *134*, 012402.
[11] X. Chen, *Surf. Coat. Technol.* **2006**, *200*, 3418.

DOI: 10.1002/adem.201500371

[12] S. Kramer, S. Faulhaber, M. Chambers, D. R. Clarke, C. G. Levi, J. W. Hutchinson, A. G. Evans, *Mat. Sci. Eng. A* **2008**, *490*, 26.
[13] P. Mohan, T. Patterson, B. Yao, Y. Sohn, *J. Therm. Spray Technol*. **2010**, *19*, 156.
[14] J. M. Drexler, A. D. Gledhill, K. Shinoda, A. L. Vasiliev, K. M. Reddy, S. Sampath, N. P. Padture, *Adv. Mat*. **2011**, *23*, 2419.
[15] A. D. Gledhill, K. M. Reddy, J. M. Drexler, K. Shinoda, S. Sampath, N. P. Padture, *Mat. Sci. Eng. A Struct. Mat. Props. Microstruct. Process*. **2011**, *528*, 7214.
[16] M. H. Vidal-Setif, N. Chellah, C. Rio, C. Sanchez, O. Lavigne, *Surf. Coat. Technol*. **2012**, *208*, 39.
[17] M. Shinozaki, T. W. Clyne, *Surf. Coat. Technol*. **2013**, *216*, 172.
[18] K. I. Lee, L. T. Wu, R. T. Wu, P. Xiao, *Surf. Coat. Technol*. **2014**, *260*, 68.
[19] J. M. Crosby, S. Lewis, J. P. Bons, W. G. Ai, T. H. Fletcher, *J. Eng. Gas Turbines Power (ASME)* **2008**, *130*, 051503.
[20] J. E. Wammack, J. Crosby, D. Fletcher, J. P. Bons, T. H. Fletcher, *J. Turbomach. (ASME)* **2008**, *130*, Article No. 021020.
[21] B. P. Casaday, A. A. Ameri, J. P. Bons, *J. Eng. Gas Turbines Power (ASME)* **2013**, *135*, Article No. 032001.
[22] M. Kostoglou, A. G. Konstandopoulos, *J. Aerosol Sci*. **2000**, *31*, 427.
[23] N. E. L. Haugen, S. Kragset, *J. Fluid Mech*. **2010**, *661*, 239.
[24] C. Bonilla, J. Webb, C. Clum, B. Casaday, E. Brewer, J. P. Bons, *J. Eng. Gas Turbines Power (ASME)* **2012**, *134*, Article No. 101901.
[25] J. W. Jensen, S. W. Squire, J. P. Bons, T. H. Fletcher, *J. Turbomach. (ASME)* **2005**, *127*, 462.
[26] J. P. Van der Walt, A. Nurickt, *J. Aircr*. **1995**, *32*, 106.
[27] W. Tabakoff, A. Hamed, M. Metwally, *J. Eng. Gas Turbines Power (ASME)* **1991**, *113*, 607.
[28] M. M. Weaver, M. G. Dunn, T. Heffernan, in *41st ASME Gas Turbine and Aeroengine Congress*. Birmingham **1996**, UK: ASME, (Eds: E. D. Larson, C. I. Marrison) p. 1.
[29] M. G. Dunn, A. J. Baran, J. Miatech, *J. Eng. Gas Turbines Power (ASME)* **1996**, *118*, 724.
[30] M. H. Vidal-Setif, C. Rio, D. Boivin, O. Lavigne, *Surf. Coat. Technol*. **2014**, *239*, 41.
[31] H. N. Yow, M. J. Pitt, A. D. Salman, *Adv. Powder Technol*. **2005**, *16*, 363.
[32] M. Le, I. Hassan, *Appl. Therm. Eng*. **2006**, *26*, 2035.
[33] F. Sharipov, *J. Phys. Chem. Ref. Data* **2011**, *40*, Article No. 023101.
[34] J. N. Chao, J. F. Lu, H. R. Yang, M. Zhang, Q. Liu, *Int. J. Heat Mass Transfer* **2015**, *80*, 115.
[35] R. A. Ricks, N. J. E. Adkins, T. W. Clyne, *Powder Metall*. **1986**, *29*, 29.
[36] G. Trapaga, E. F. Matthys, J. J. Valencia, J. Szekely, *Met. Trans. B - Proc. Met*. **1992**, *23*, 701.
[37] Z. Zhao, D. Poulikakos, J. Fukai, *Int. J. Heat Mass Transfer*, **1996** *39*, 2771.
[38] H. Tabbara, S. Gu, *Appl. Phys. A Mater. Sci. Process*. **2011**, *104*, 1011.
[39] E. Meillot, S. Vincent, C. Le Bot, F. Sarret, J. P. Caltagirone, L. Bianchi, *Surf. Coat. Technol*. **2015**, *268*, 257.
[40] C. Le Bot, S. Vincent, E. Meillot, F. Sarret, J. P. Caltagirone, L. Bianchi, *Surf. Coat. Technol*. **2015**, *268*, 272.
[41] Z. H. Zhu, S. Kamnis, S. Gu, *Acta Mater*. **2015**, *90*, 77.